Particuology 115 (2026) 401–414

Contents lists available at ScienceDirect

Particuology

journal homepage: www.elsevier.com/locate/partic

Ultrasound-assisted negative pressure crystallization of ammonium sulfate: Synergistic effects and intensification mechanisms

Qian Zhang[a,b], Guang Fu[c], Shuo Xu[b], Dongbin Wang[a,b], Thiquynhxuan Le[a,b,*], Libo Zhang[a,b,**]

[a] State Key Laboratory of Complex Non-ferrous Metal Resources Clean Utilization, Kunming University of Science and Technology, Kunming, 650093, China
[b] Faculty of Metallurgical and Energy Engineering, Kunming University of Science and Technology, Kunming, 650093, China
[c] Yunnan Chihong Zinc and Germanium Co., Ltd., Qujing, 655011, China

HIGHLIGHTS

- Ultrasound-assisted negative pressure crystallization of ammonium sulfate solution.
- Yield increased by 27.64 g and direct yield improved by 36.80% compared to negative pressure crystallization.
- MSZW narrowed by 33%, solid-liquid transition time shortened by 35.7%, and solution viscosity reduced by 5.7%.
- Crystals with more uniform size, regular morphology, and enhanced crystallinity are obtained.

GRAPHICAL ABSTRACT

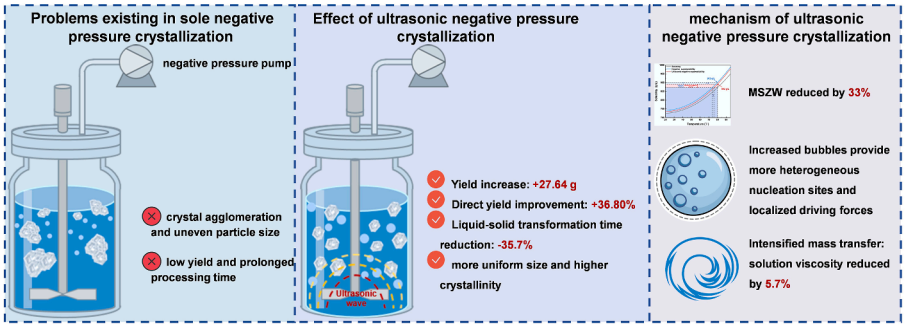

ARTICLE INFO

Keywords:
Ultrasound
Negative pressure crystallization
Synergistic intensification
Ammonium sulfate

ABSTRACT

Although negative pressure crystallization of ammonium sulfate can mitigate low yield and long processing time in atmospheric pressure crystallization, it still faces challenges in enhancing crystallization efficiency and achieving a uniform crystal size distribution. To address these issues, this study proposed an ultrasound-assisted negative pressure crystallization technique. Under optimized conditions (pH = 7, 300 rpm, 80 °C, 45 min, 180 W, 0.03 MPa), the yield increased by 27.64 g and the direct yield improved by 36.80% compared with negative pressure crystallization. XRD and FTIR confirmed that this process maintained the crystal structure of ammonium sulfate while enhancing crystallinity. Mechanistic studies revealed that, compared with negative pressure crystallization, the synergistic effect of ultrasound narrowed the metastable zone width (MSZW) by approximately 33%, lowering the nucleation energy barrier. Ultrasound cavitation generated numerous bubbles, providing heterogeneous nucleation sites and localized supersaturation driving forces, which jointly accelerated nucleation and reduced the solid-liquid transition time by 35.7%. Furthermore, compared with the negative pressure crystallization system, the ultrasonic negative pressure crystallization reduced the solution viscosity by 5.7%, enhancing mass transfer and crystal growth. Ultimately, ultrasound-assisted negative pressure crystallization

* Corresponding author. State Key Laboratory of Complex Non-ferrous Metal Resources Clean Utilization, Kunming University of Science and Technology, Kunming, 650093, China.
** Corresponding author. State Key Laboratory of Complex Non-ferrous Metal Resources Clean Utilization, Kunming University of Science and Technology, Kunming, 650093, China.
E-mail addresses: quynhxuanlt@kust.edu.cn (T. Le), zhanglibopaper@126.com (L. Zhang).

https://doi.org/10.1016/j.partic.2026.06.003
Received 7 April 2026; Received in revised form 6 May 2026; Accepted 6 June 2026
Available online 9 June 2026

produced crystals with more uniform size and more regular morphology, offering important theoretical insights for improving ammonium sulfate crystallization processes.

1. Introduction

Ammonium sulfate ($(NH_4)_2SO_4$), as an important chemical product, has been widely applied in agriculture (Yan et al., 2024), rare earth extraction (Wang et al., 2024), food processing (Edward et al., 2023), battery materials (Qu et al., 2022), and resource recovery (Yang et al., 2025), possessing significant value. Among the production methods of ammonium sulfate, the ammonia-based flue gas desulfurization technology exhibits distinct environmental protection and resource utilization advantages, as it converts sulfur dioxide in smelting flue gas into ammonium sulfate product, achieving efficient utilization of sulfur resources (Peng et al., 2024). The ammonia-based desulfurization process mainly comprises the following steps: smelting flue gas enters the desulfurization tower where it contacts and reacts with ammonia water (the desulfurizing agent) to generate ammonium sulfite. Subsequently, under the action of oxidants (such as concentrated sulfuric acid, oxygen, or compressed air), ammonium sulfite is oxidized to ammonium sulfate solution. Finally, ammonium sulfate solid product is obtained through the crystallization process (Xu et al., 2024). Among these, the crystallization process serves as a critical step controlling product particle size and yield, exerting an important influence on the quality and application performance of the final product.

Currently, industrial crystallization methods used for ammonium sulfate include atmospheric evaporative crystallization (Peng et al., 2024) and cooling crystallization (Shao et al., 2022). Although cooling crystallization features relatively simple operation and low energy consumption, it commonly suffers from problems such as uneven supersaturation distribution and insufficient crystallization driving force due to limited heat transfer efficiency, leading to slow crystallization rate, prolonged crystallization cycle, and low product yield. In contrast, atmospheric evaporative crystallization maintains stable supersaturation through continuous solvent evaporation, enabling relatively continuous nucleation and growth, thereby significantly enhancing product yield and production efficiency; consequently, it has become the current mainstream process. However, the elevated operating temperature intensifies molecular thermal motion, readily inducing secondary nucleation and crystal fragmentation, which results in broadened particle size distribution and irregular crystal morphology. Moreover, the high latent heat of evaporation entails considerable energy consumption, indicating substantial room for improving crystallization efficiency. To improve evaporative crystallization performance, industrial processes often employ intensification methods such as seed addition or negative pressure evaporation. Seed addition provides pre-existing growth interfaces and reduces the nucleation free energy barrier, thereby suppressing primary nucleation and directing crystal growth. Nevertheless, the dosage and timing of seed addition must be precisely aligned with the supersaturation evolution trajectory, resulting in an extremely narrow operational window and significant challenges in industrial controllability. Negative pressure crystallization reduces the boiling point of the solution by lowering the system pressure, enabling solvent evaporation at lower temperatures, which offers benefits in energy saving and thermal-sensitive material protection. However, the abrupt pressure drop frequently induces solvent flash evaporation, causing a sharp surge in supersaturation within an extremely short timeframe. This readily drives the system beyond the metastable zone, triggering burst nucleation and generating excessive fine crystals accompanied by severe agglomeration, ultimately leading to broad particle size distribution, poor uniformity, and substantially increased burden on subsequent filtration and drying operations. Therefore, developing novel crystallization processes capable of overcoming the limitations of existing technologies holds significant importance for achieving efficient cyclic utilization of sulfur resources in the ammonia-based desulfurization process.

Ultrasound is a mechanical wave with frequency greater than 20 kHz, possessing unique mechanical effects, cavitation effects, etc. (Devos et al., 2025; Ileri et al., 2015), and has been proven to effectively intensify the crystallization process. Studies have shown that ultrasound can effectively reduce diffusion resistance, enhance mass transfer, and promote the formation of crystal nuclei. In atmospheric pressure crystallization, it can increase nucleation rate, shorten solid-liquid transition time, and make crystal particle size distribution more concentrated and morphology more regular. For example, Zhong et al. (Zhong et al., 2022) investigated the effect of ultrasound on the anti-solvent crystallization kinetics of sucrose, finding that the introduction of ultrasound could significantly increase the kinetic constant of nucleation rate from 9.76×10^2 to 8.38×10^8. Hu et al. (Hu et al., 2006) introduced ultrasound into sucrose evaporative crystallization, discovering that while reducing sugar solution viscosity, the heat transfer coefficient and evaporation intensity increased by 42.4% and 15.2%, respectively. For ammonium sulfate evaporative crystallization, our previous research (Xu et al., 2024) indicated that under atmospheric pressure, the introduction of ultrasound could shorten the solid-liquid transition time by 10%. Furthermore, ultrasound can also make crystal particle size distribution more uniform and crystal form more perfect. Dong et al. (2025) studied the effect of ultrasound on the crystallization process of xylene, finding that the introduction of ultrasound could increase crystal roundness by 21.6%–27.7%, while reducing fractal dimension by 6.98%–11.2%. Mohod and Gogate (2018) compared conventional crystallization with ultrasound-assisted crystallization, discovering that ammonium sulfate crystals with smaller size, uniform particle size, smooth surface, and regular edges could be obtained under ultrasound action. These studies all demonstrate that ultrasound can effectively intensify the nucleation and growth stages of the crystallization process, improving product characteristics. Combining ultrasound with negative pressure is expected to form complementary advantages, synergistically solving problems such as low yield and broad particle size distribution existing in current negative pressure crystallization. Preliminary studies have shown that ultrasound-negative pressure coupling technology has demonstrated potential in enhancing extraction efficiency and improving particle size distribution in other fields. For instance, Min et al. (2022) studied the extraction of paclitaxel from *Taxus chinensis* under ultrasound-negative pressure conditions and found that, in only 3–8 min, paclitaxel yield could reach 94–100%. Li et al. (2022) investigated the effect of negative pressure combined with ultrasound treatment on the fine structure of rice starch, discovering that the average particle size of rice starch decreased and the distribution range narrowed after treatment. This provides reference for ammonium sulfate crystallization under ultrasound-assisted negative pressure.

Based on this, in response to the deficiencies of existing ammonium sulfate negative pressure crystallization processes, including low product yield, uneven particle size distribution, and irregular crystal morphology, this study developed a novel ultrasound-assisted negative pressure crystallization process. The effects of different reaction conditions on ammonium sulfate crystallization yield and direct yield were investigated, and process parameters were optimized. Through comparison with atmospheric evaporation, ultrasound-assisted atmospheric evaporation, and negative pressure evaporation crystallization, the mechanism of action of ultrasound-assisted negative pressure on the ammonium sulfate crystallization process was elucidated, with the aim of providing new directions for the upgrading of industrial crystallization processes.

2. Experimental

2.1. Materials and equipment

The ammonium sulfate used in this experiment was purchased from Tianjin Zhiyuan Chemical Reagent Co., Ltd. (AR grade). Deionized water (H_2O) used in the experiment was prepared by an ultrapure water system. The ultrasound and stirring equipment selected was self-developed by the Key Laboratory of Unconventional Metallurgy, Ministry of Education, Kunming University of Science and Technology. The operating frequency of the ultrasound equipment was fixed at 40 kHz, with ultrasonic waves emitted vertically upward from the bottom. The actual power was controlled by adjusting the output power percentage, with a maximum output of 300 W. The stirring speed ranged from 100 to 2000 rpm.

2.2. Experimental procedure

75 g of ammonium sulfate was dissolved in 110 mL deionized water with continuous stirring until complete dissolution to prepare a saturated ammonium sulfate solution simulating industrial concentration. The solution was then transferred to a 250 mL three-neck round-bottom flask and subjected to negative pressure (vacuum degree) evaporative crystallization in an ultrasound reactor. The solution temperature was monitored in real time by a PT100 sensor and maintained at the set value using an MCH heating plate and a circulating water bath (accuracy ±0.5 °C). After reaching the predetermined crystallization time, the reaction was terminated and the mixture was subjected to solid-liquid separation. The obtained ammonium sulfate crystals were washed with anhydrous ethanol to remove residual mother liquor on the surface, dried at 65 °C for 12 h to obtain ammonium sulfate solid, weighed and recorded for crystallization yield, and the direct yield was calculated according to Eq. (1). Each experiment was repeated three times independently. The samples were sealed and stored for subsequent use. The experimental flowchart is shown in Fig. 1. All experiments were conducted using a one-factor-at-a-time design, where each operational parameter was varied individually while keeping others constant. These experiments were performed under basic conditions (initial pH = 7) to investigate the effects of key operating parameters including different stirring speeds, temperatures, times, ultrasonic powers (set power), and negative pressure intensities on ammonium sulfate yield and direct yield, and to compare the differences between ultrasonic negative pressure and sole negative pressure crystallization systems.

$$f = \frac{m_1}{m_0} \times 100\% \quad (1)$$

where f is the direct yield, m_1 is the actual yield of ammonium sulfate (g), and m_0 is the total mass of ammonium sulfate initially dissolved in the solution (75 g).

In this study, the metastable zone of ammonium sulfate was determined by measuring its solubility and supersolubility. First, the solubility was measured using the isothermal dissolution equilibrium method. At each target temperature, excess ammonium sulfate was added to distilled water in batches until supersaturation was reached. After constant temperature stirring for 30 min to achieve solid-liquid equilibrium, a quantitative amount of saturated supernatant was taken, evaporated to dryness, and weighed to calculate the solubility. The supersolubility was determined under the same temperature system by applying constant negative pressure to the saturated solution to promote solvent evaporation. The solution was closely observed until crystal nuclei first appeared, at which point the process was immediately stopped. The amount of evaporated water was recorded to calculate the supersolubility at that temperature. To investigate the effect under ultrasound-negative pressure conditions, the bottom ultrasound was turned on simultaneously with the application of negative pressure (other operations remained consistent), and the supersolubility curve under ultrasound conditions was determined. Finally, the metastable zone width (MSZW) of the system was defined by the solubility and supersolubility at the same temperature.

2.3. Analysis methods

The crystal structure and crystallinity of ammonium sulfate were analyzed by an X-ray diffractometer (XRD, Rigaku Miniflex 600, Japan) and Fourier transform infrared spectrometer (FTIR, Thermo Fisher Scientific Nicolet iS20, USA). The crystallinity is calculated as the percentage of the integrated area of XRD crystalline diffraction peaks to the total scattering area. The crystal morphology and particle size distribution of ammonium sulfate were characterized by scanning electron microscope (SEM, ZEISS Sigma 300, Germany) and laser particle size analyzer (Mastersizer 2000, UK). The viscosity of ammonium sulfate solution was measured by rotational viscometer (NDJ-9SE, China). The effects of different conditions on crystal growth were observed using a scanning electron microscope (SEM, ZEISS Sigma 300, Germany).

3. Results and discussions

3.1. Effect of ultrasonic negative pressure on ammonium sulfate crystallization

3.1.1. Effect of stirring speed

Under the conditions of initial pH = 7, crystallization temperature of 80 °C, ultrasound time of 45 min, and negative pressure level of 0.03 MPa, the effects of different stirring speeds (0, 100, 200, 300, and 400 rpm) on the yield and direct yield of ammonium sulfate were investigated for both sole negative pressure and ultrasonic (120 W) negative pressure crystallization conditions. The results are shown in Fig. 2.

With the increase of stirring speed, the crystallization yield and

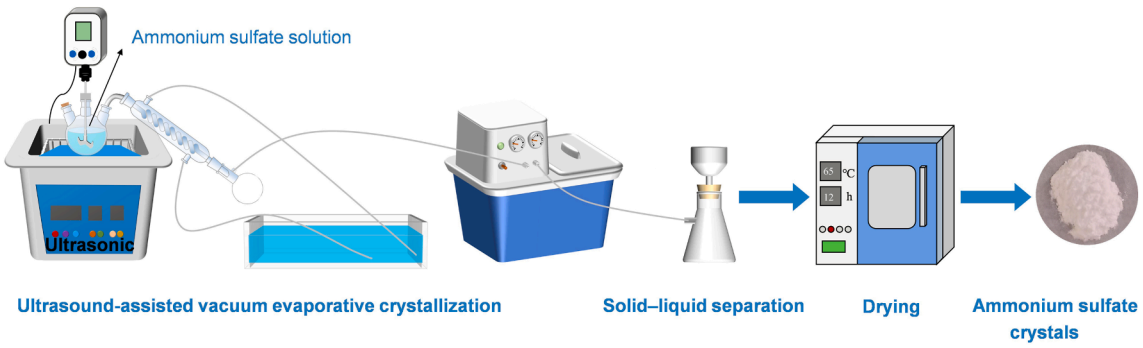

Fig. 1. Schematic of the experimental procedure.

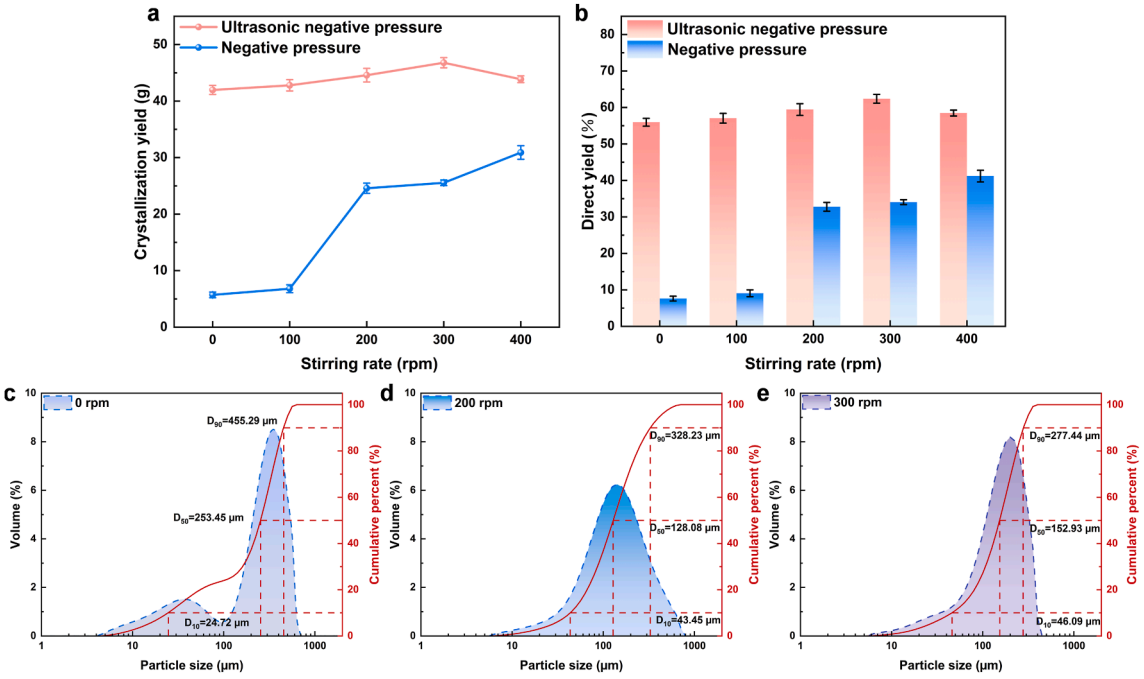

Fig. 2. Effect of stirring speed on (a) crystallization yield and (b) direct yield of ammonium sulfate in ultrasonic negative pressure and sole negative pressure systems; and product particle size distribution under ultrasonic negative pressure conditions at (c) 0 rpm, (d) 200 rpm, and (e) 300 rpm.

direct yield of ammonium sulfate under ultrasonic negative pressure conditions showed a trend of first increasing and then decreasing, while those in the sole negative pressure system increased monotonically. Under ultrasonic negative pressure crystallization conditions, the crystallization yield and direct yield continuously improved as the stirring speed increased from 0 rpm to 300 rpm. Moderate intensification of stirring enhances solution mixing and molecular collision, thereby promoting the establishment of supersaturation, reducing nucleation energy barrier, and accelerating nucleation rate (Zheng et al., 2023). However, excessively high stirring speed induces multiple adverse effects. Specifically, intensified crystal-impeller collisions lead to crystal wear and fragmentation, triggering secondary nucleation and partial dissolution; disturbance of the ultrasonic field distribution weakens cavitation intensity and diminishes the nucleation-promoting effect of ultrasound; meanwhile, liquid splashing causes fine crystals to adhere to the vessel wall above the liquid surface, reducing crystal nuclei in the liquid phase (Mohod & Gogate, 2018). This combined effect inhibits the crystallization process, and ultimately decreases the yield and direct yield of ammonium sulfate. Therefore, when the stirring speed increased to 400 rpm, the yield and direct yield of ammonium sulfate decreased. In contrast, in the sole negative pressure crystallization system, due to the lower mass transfer rate, the increase of stirring speed (within the range investigated in this experiment) continuously improved the mixing effect, resulting in a monotonic upward trend of yield and direct yield of ammonium sulfate.

In the ultrasonic negative pressure crystallization system, stirring speed also had an important influence on product particle size distribution. A moderately increased stirring speed enhances the mixing effect of the crystallization system, inhibits local supersaturation phenomena, and prevents the formation of large crystal particles, thereby yielding products with smaller particle size and narrower distribution (Fig. 2 (c–e)). Under static conditions (0 rpm), uneven solute distribution led to unbalanced nucleation sites and large differences in crystal grain size; under lower stirring speed (200 rpm) conditions, problems such as uneven local supersaturation distribution caused by insufficient solute mixing still existed, resulting in broad particle size distribution and poor convergence. In contrast, moderate stirring (300 rpm) reduced concentration gradients, inhibited particle aggregation, and decreased product particle size. Therefore, in the ultrasonic negative pressure crystallization system, 300 rpm is selected as the optimal stirring speed.

3.1.2. *Effect of temperature*

Under the conditions of initial pH = 7, stirring speed of 300 rpm, crystallization time of 45 min, and negative pressure level of 0.03 MPa, the effects of different temperatures (50, 60, 70, 80, and 90 °C) on the crystallization yield and direct yield of ammonium sulfate were investigated for both sole negative pressure and ultrasonic (120 W) negative pressure crystallization conditions. The results are shown in Fig. 3.

Increasing temperature exhibited a positive promoting effect on both the crystallization yield and direct yield in the two systems. Under ultrasonic negative pressure conditions, when the temperature increased from 50 to 80 °C, the crystallization yield of ammonium sulfate increased from 17.91 to 46.78 g, and the direct yield improved by 38.49%. The enhancement mechanism is as follows: first, the increase in temperature directly elevates the supersaturation of the solution, providing a key thermodynamic driving force for nucleation and crystal growth. Second, rising temperature causes a decrease in liquid surface tension and an increase in vapor pressure inside cavitation bubbles, reducing the cavitation threshold and thereby facilitating bubble formation (Wang et al., 2025). According to surface energy theory, the gas-liquid interface can serve as a low-barrier nucleation site; meanwhile, the local hot spots generated by bubble collapse cause instantaneous solvent vaporization and a sudden increase in local supersaturation, inducing primary nucleation (Vishwakarma & Gogate, 2017). Furthermore, the temperature increase directly affects the amount of solvent evaporated. As shown in Fig. 3(c), the amount of solvent evaporated within a fixed crystallization time of 45 min increases sharply with temperature in both the negative pressure and ultrasonic negative pressure systems. Penha et al. (Penha et al., 2018) demonstrated that for highly soluble inorganic salts, even a slight evaporation of solvent can rapidly concentrate the solution, thereby inducing substantial solute crystallization. The synergistic effect of the above multiple mechanisms collectively achieved a significant increase in the yield of ammonium sulfate. When the temperature further increased to 90 °C, the crystallization yield of ultrasonic negative pressure only increased by 2.53 g, and the direct yield only improved by

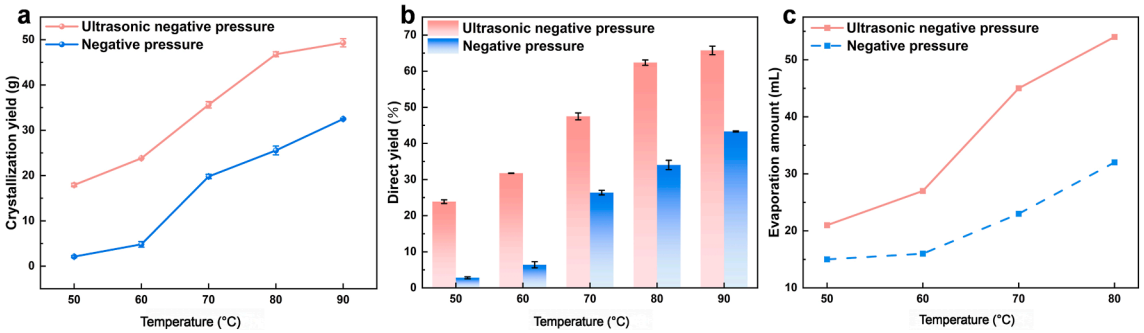

Fig. 3. Effect of temperature on (a) crystallization yield, (b) direct yield of ammonium sulfate in ultrasonic negative pressure and sole negative pressure systems, and (c) evaporated water amount at different temperatures.

3.38%, with the growth rate significantly weakening. When the temperature exceeds 80 °C, the promoting effect of temperature on crystallization tends to saturate. As the temperature rises, the saturated vapor pressure of water increases significantly, reaching 31.2, 47.4, and 70.1 kPa at 70, 80, and 90 °C, respectively, with the increment from 80 to 90 °C being 1.4 times that from 70 to 80 °C. The rapid increase of vapor pressure at high temperatures causes a large number of water vapor molecules to diffuse into cavitation bubbles. Pei et al. (2025) reported that over-expansion of the primary bubble reduces the local pressure below the critical threshold for cavitation nucleation, thereby inducing new small bubbles. These small bubbles coalesce with the primary bubble, leading to surface destabilization and promoting bubble fission, which further weakens the collapse intensity. Meanwhile, the excessive number of cavitation bubbles becomes densely distributed, forming cavitation clouds where mutual energy cancellation further diminishes the overall cavitation effect (Xu et al., 2024). The balance between the positive and negative effects occurs at 80 °C, and therefore the crystallization effect is optimal at this temperature. This trend is consistent with the temperature effect on nano-ZnO crystallization reported by Guo et al. (2026), whose study also confirms that 80 °C represents the optimal balance between cavitation-assisted mass-transfer enhancement and accelerated reaction kinetics. Considering marginal benefit and energy consumption for heating comprehensively, 80 °C is selected as the optimal crystallization temperature for ammonium sulfate under ultrasonic negative pressure.

In contrast, the yield and direct yield of the sole negative pressure crystallization system also increased with rising temperature. This is because in the negative pressure crystallization system, heating only accelerates water evaporation by increasing the average kinetic energy of molecules (Aquilanti et al., 2018) and reducing solution viscosity, thereby slowly promoting the formation of supersaturation, resulting in limited crystallization efficiency. Therefore, at the same temperatures, the yield and direct yield were significantly lower than those of the ultrasonic negative pressure system.

3.1.3. *Effect of time*

Under the conditions of initial pH = 7, stirring speed of 300 rpm, crystallization temperature of 80 °C, and negative pressure level of 0.03 MPa, the effects of different times (25, 35, 45, and 55 min) on the crystallization yield and direct yield of ammonium sulfate were investigated for both sole negative pressure and ultrasonic (120 W) negative pressure crystallization conditions. The results are shown in Fig. 4.

Extending the time improved the crystallization yield of both systems, but the ultrasonic negative pressure system exhibited higher crystallization efficiency within the same time period. In the ultrasonic negative pressure system, when the ultrasound time was short (<35 min), the energy input was insufficient to overcome the crystallization energy barrier, and the cavitation effect failed to fully promote nucleation and mass transfer, resulting in insufficient nucleation and low yield (Xu et al., 2025). Extending the ultrasound time to 45 min significantly enhanced the cavitation effect, continuously promoted mass transfer and nucleation, and significantly increased the yield to 46.78 g. Further extension to 55 min only resulted in a slight increase of 1.64 g in yield and 2.19% in direct yield, indicating that the crystallization process was approaching equilibrium. Considering that excessively long ultrasound time increases time costs and may cause excessive fragmentation of ammonium sulfate particles due to strong ultrasonic cavitation effects, leading to problems such as easy caking, poor flowability, and increased powder loss in practical applications, 45 min is selected as the optimal crystallization time. In the sole negative pressure system, extending time could also increase crystallization amount by continuously evaporating solvent to improve supersaturation, but its growth rate was lower than that of the ultrasonic negative pressure system. A comparison of the two systems revealed that the introduction

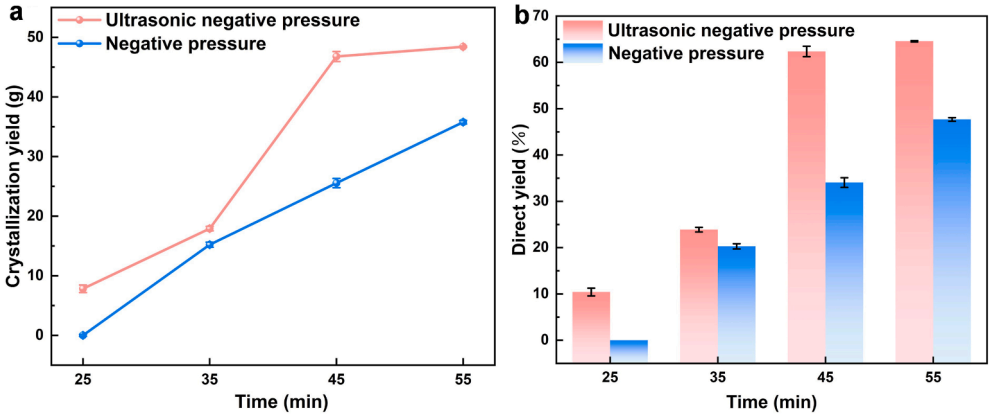

Fig. 4. Effect of time on (a) crystallization yield and (b) direct yield of ammonium sulfate in ultrasonic negative pressure and sole negative pressure systems.

of ultrasound significantly shortened the time required to achieve the same yield and improved the efficiency of the crystallization process.

3.1.4. Effect of ultrasonic power

Under the conditions of initial pH = 7, stirring speed of 300 rpm, crystallization temperature of 80 °C, ultrasound time of 45 min, and negative pressure level of 0.03 MPa, the effects of different ultrasonic powers (60, 120, 180, and 240 W) on the crystallization yield and direct yield of ammonium sulfate were investigated under ultrasonic negative pressure crystallization conditions. The results are shown in Fig. 5.

With the increase of ultrasonic power, the crystallization yield and direct yield of ammonium sulfate showed a trend of initial increase followed by a decrease. When the ultrasonic power increased from 60 to 180 W, crystallization yield rose from 29.23 to 53.18 g and the direct yield increased from 38.97% to 70.91%. This was attributed to the fact that higher power input induced stronger cavitation effects, high-speed micro-jets, and shock waves, which effectively thinned the diffusion boundary layer on the crystal surface, accelerated the transport of solute to the crystal faces, and thereby enhanced the mass transfer process (Yang et al., 2023). Furthermore, as the ultrasonic power increases, the generation rate and number of cavitation bubbles increase significantly (Gao et al., 2022; Seo & Lee, 2023). The gas-liquid interfaces of these bubbles provide abundant heterogeneous nucleation sites, which lower the critical nucleation energy barrier and thereby promote primary nucleation (Zhao et al., 2023). Meanwhile, the intense micro-turbulence and high-frequency vibrations generated by ultrasound can disrupt solute molecular clusters and aggregates, increasing the number of free solute molecules available for crystal growth (Song et al., 2023). These synergistic effects collectively contribute to the remarkable enhancement in crystallization yield and direct yield. However, further increasing the ultrasonic power to 240 W resulted in a decrease in yield to 30.43 g and direct yield to 40.57%. This was ascribed to the excessive ultrasonic intensity, which induced intense turbulence and shear, causing excessive fragmentation of crystals and generating a large number of fine secondary nuclei. The newly generated fine crystals competed with primary nuclei for solute, inhibiting crystal growth rate and even causing partial re-dissolution of the already formed crystals, ultimately leading to decreased yield (Wang et al., 2025). Therefore, 180 W is selected as the optimal condition.

3.1.5. Effect of negative pressure

Under the conditions of initial pH = 7, stirring speed of 300 rpm, crystallization temperature of 80 °C, crystallization time of 45 min, and ultrasonic power of 180 W, the effects of different negative pressure intensities (0.01, 0.02, 0.03, and 0.04 MPa) on the crystallization yield and direct yield of ammonium sulfate were investigated under ultrasonic negative pressure crystallization conditions. The results are shown in Fig. 6(a and b).

Negative pressure mainly enhanced the crystallization process by lowering the boiling point of the solvent and accelerating evaporation, exhibiting a synergistic effect with ultrasound. Under the same negative pressure conditions, the introduction of ultrasound significantly improved the crystallization yield and direct yield of ammonium sulfate compared with sole negative pressure crystallization. When the negative pressure level was increased from 0.01 to 0.03 MPa, under ultrasonic negative pressure crystallization conditions, the crystallization yield increased from 41.28 to 53.18 g, and the direct yield improved from 55.04% to 70.90%; while the maximum yield in the sole negative pressure crystallization system was only 25.54 g with a direct yield of 34.1%. Regardless of whether ultrasound was applied, the enhancement of negative pressure promoted efficient evaporation of the solution at lower temperatures by reducing the boiling point of the solvent, accelerating supersaturation accumulation and shortening the nucleation induction period (Kim et al., 2026). As shown in Fig. 6(c), under the ultrasonic negative pressure condition, the amount of water evaporation increased with increasing negative pressure, thereby providing a stronger thermodynamic driving force for sustained crystal precipitation and improving the crystallization yield and direct yield. However, when the negative pressure exceeded 0.03 MPa, both the crystallization yield and direct yield of the two systems exhibited a decreasing trend. This was because excessively strong negative pressure caused overly rapid solvent evaporation (Liu et al., 2024), causing the supersaturation of the system to prematurely exceed the metastable zone, which readily induced burst nucleation. Meanwhile, vigorous boiling reduced the suspension stability of crystals, with some even being carried into the evaporation zone or attached to the vessel wall, resulting in reduced effective crystallization amount. Furthermore, excessively high negative pressure caused overly rapid evaporation and substantial absorption of latent heat, leading to a drop in solution temperature. This increased the solution viscosity and inhibited crystal growth; most crystals thus became too fine to be recovered efficiently, further reducing the actual yield (Liu et al., 2015).

In terms of crystal particle size, Fig. 6(d and e) showed that under both negative pressure and ultrasonic negative pressure conditions, D50 first increased and then decreased with increasing negative pressure level, and the particle size distribution was narrowest and the particle size was most uniform when the negative pressure level was 0.03 MPa. Comparison of SEM images in Fig. 6 revealed that the negative pressure level had little effect on crystal morphology. Therefore, 0.03 MPa is selected as the optimal negative pressure level.

In summary, under the condition of initial pH = 7, the optimal process parameters for ultrasound-assisted negative pressure crystallization were as follows: stirring speed of 300 rpm, crystallization temperature of 80 °C, crystallization time of 45 min, ultrasonic power of 180 W, and negative pressure level of 0.03 MPa. Under these conditions, the crystallization yield of ammonium sulfate was 53.18 g with a direct

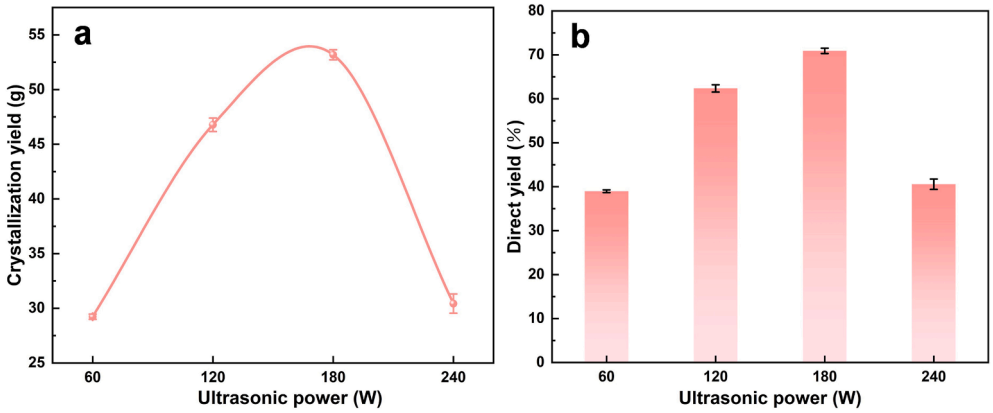

Fig. 5. Effect of ultrasonic power on ammonium sulfate crystallization under negative pressure conditions: (a) crystallization yield and (b) direct yield.

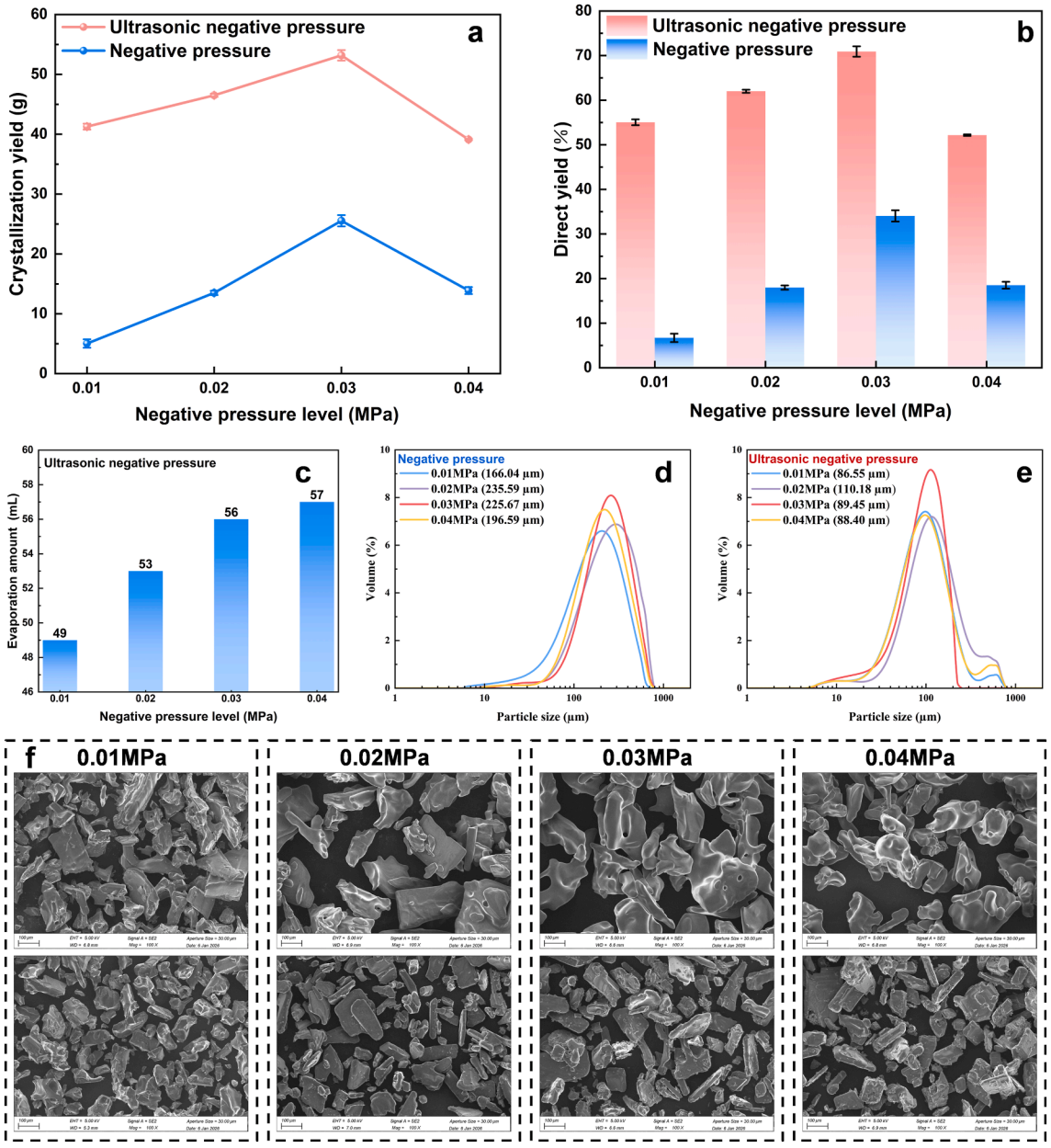

Fig. 6. Effect of negative pressure level on ammonium sulfate crystallization: (a) yield, (b) direct yield, (c) evaporated water amount under ultrasonic negative pressure, (d) particle size distribution (including D50) under negative pressure, (e) particle size distribution (including D50) under ultrasonic negative pressure, (f) crystallization morphologies (top row: negative pressure, bottom row: ultrasonic negative pressure).

yield of 70.9%. Among the five parameters, excluding time (which is not an operational variable), temperature and ultrasonic power were identified as the primary drivers for improving crystallization performance, as they contributed the largest increases in yield.

3.2. *Mechanism of ultrasound-assisted vacuum crystallization enhancement*

3.2.1. *Comparison of crystallization products under different conditions*

Under the conditions of initial pH = 7, stirring speed of 300 rpm, crystallization temperature of 80 °C, and crystallization time of 45 min, the effects of four processing conditions on the crystallization yield and direct yield of ammonium sulfate were compared: conventional crystallization (0 W, ambient pressure), ultrasonic crystallization (180 W, ambient pressure), negative pressure crystallization (0 W, 0.03 MPa), and ultrasonic negative pressure crystallization (180 W, 0.03 MPa), as shown in Fig. 7(a). Among these, conventional crystallization did not yield any crystals within 45 min, and the reaction was extended to 120 min to obtain comparable products. The other three conditions were all maintained at 45 min. The XRD patterns, FTIR spectra, SEM images, and particle size distributions of the four ammonium sulfate products are shown in Fig. 7(b), (c), (d), and (e), respectively, and the calculated crystallinity of these products is presented in Table 1.

As shown in Fig. 7(a), the crystallization yield under ultrasonic negative pressure conditions was 53.18, 27.64 and 50.47 g higher than those of conventional, ultrasonic, and negative pressure crystallization, respectively, corresponding to direct yield improvements of 70.90%, 36.80%, and 67.29%. These results clearly demonstrate the synergistic enhancement effect of ultrasound and negative pressure. The XRD patterns (Fig. 7(b)) showed that in the ultrasonic negative pressure crystallization process, the diffraction of (020), (120), (040) and other crystal planes was enhanced, with significantly improved overall peak

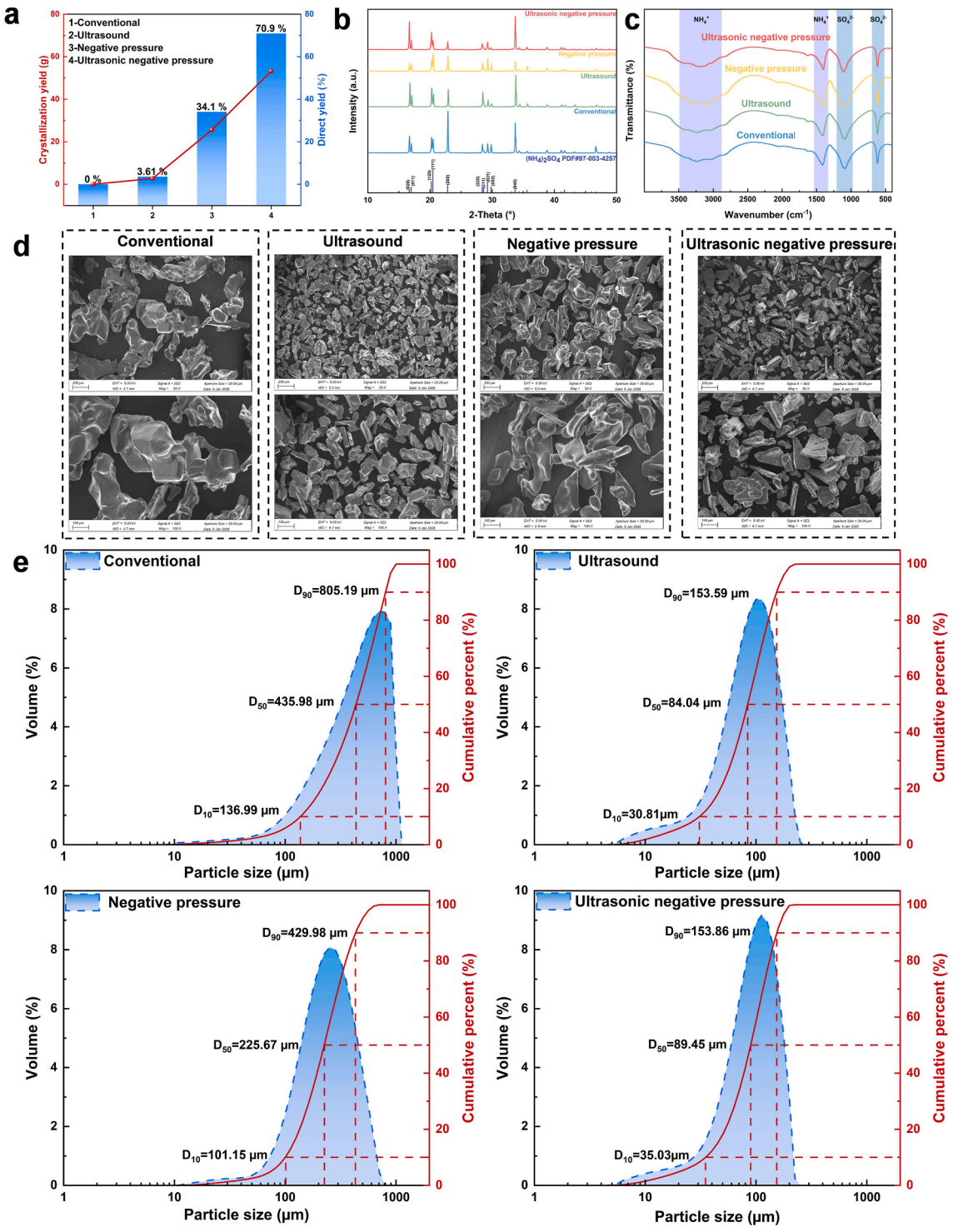

Fig. 7. Crystallization yield and direct yield (a), XRD patterns (b), FTIR spectra (c), SEM images (d), and particle size distribution (e) of ammonium sulfate prepared under conventional, ultrasonic, negative pressure, and ultrasonic negative pressure conditions.

intensity, indicating that the ultrasonic negative pressure crystallization method was conducive to crystal growth along specific directions. Moreover, as shown in Table 1, conventional crystallization (120 min) gave the highest crystallinity (78.65%), which is attributed to its longer crystallization time that allowed for sufficient grain growth and orderly lattice arrangement. However, within the same crystallization time (45 min), the crystallinity under negative pressure was 72.72%, while under ultrasonic negative pressure it increased to 74.25%; ultrasonic crystallization alone (73.32%) was also higher than that of negative pressure crystallization. Therefore, ultrasonic assistance is beneficial for improving crystallinity. The FTIR spectra (Fig. 7(c)) indicated that the characteristic absorption peak positions of ammonium sulfate products under various conditions were consistent. Among them, the absorption peaks near 1100 cm^{-1} and 630 cm^{-1} were attributed to the v_3 asymmetric stretching vibration and v_4 bending vibration of SO_4^{2-}, respectively; the broad peak at 2800-3400 cm^{-1} and the absorption peak near 1400 cm^{-1} were attributed to the v_3 asymmetric stretching vibration and v_4 bending vibration of NH_4^+, respectively (Weis & Ewing, 1996). No

Table 1
Crystallinity of ammonium sulfate under different conditions.

Processing condition	Crystallinity (%)
Conventional (120 min)	78.65
Ultrasonic (180 W, ambient pressure, 45 min)	73.32
Negative pressure (0.03 MPa, 45 min)	72.72
Ultrasonic negative pressure (180 W, 0.03 MPa, 45 min)	74.25

Note: Crystallinity = (integral area of crystalline peaks)/(total scattering area) × 100%.

new characteristic peaks appeared in the spectra, and no original absorption peaks disappeared, which indicated that ultrasonic negative pressure did not change the molecular structure of ammonium sulfate, but promoted the crystallization process through physical effects. The SEM and particle size distribution results (Fig. 7(d and e)) further revealed that ammonium sulfate particles obtained by conventional crystallization or negative pressure crystallization showed irregular agglomeration with broad particle size distribution, while the introduction of ultrasound (alone or synergized with negative pressure) resulted in relatively more regular crystal shapes and narrower particle size distribution, indicating that ultrasound helped inhibit agglomeration and promoted uniform nucleation and growth.

3.2.2. *Ultrasonic negative pressure treatment reduces width of MSZWs*

The metastable zone width (MSZW) refers to the range of supersaturated concentration or temperature that a solution can maintain stably without spontaneous crystallization after reaching saturation, which is a key parameter for controlling the yield, crystal quality, and morphology of crystallization products (Kocks et al., 2021). In this study, the isothermal method was employed to investigate the supersaturation evolution and metastable zone width variation of ammonium sulfate solution during negative pressure crystallization and ultrasonic negative pressure crystallization processes. Based on experimental data, MSZW was quantitatively characterized, and the MSZW of ammonium sulfate crystallization under negative pressure and ultrasonic negative pressure conditions is shown in Fig. 8.

When comparing the metastable zone width of negative pressure crystallization and ultrasonic negative pressure crystallization under the same conditions, the MSZW under ultrasonic negative pressure decreased by approximately 33% compared with negative pressure crystallization, with the supersaturation concentration decreasing from 902 to 892 g/L at 80 °C. This indicates that the introduction of ultrasound reduces the stability of the supersaturated solution, making crystallization more likely to occur. This is because when ultrasonic cavitation bubbles collapse, a large amount of energy is released near the collapse point. The thermal motion of solute molecules is enhanced by this energy, increasing the bulk free energy of clusters and reducing the nucleation energy barrier of critical nuclei (Xing et al., 2026), making nucleation easier to occur and resulting in a narrower MSZW. Meanwhile, the negative pressure environment not only lowers the boiling point of the solution and accelerates solvent evaporation but also enhances cavitation intensity by reducing the hydrostatic pressure of the liquid phase. This synergistic effect enables the system to overcome the nucleation energy barrier and induce crystal precipitation at lower supersaturation levels.

3.2.3. *Enhanced nucleation and growth*

Nucleation is the initial stage of the crystallization process, essentially being the process in which crystal nuclei precipitate from supersaturated mother liquor (Myerson et al., 2019). The initial nuclei density directly determines the yield, particle size, and morphology of the final product. In this process, bubbles in the crystallization system can effectively reduce the nucleation energy barrier and promote nuclei formation by providing heterogeneous nucleation interfaces and intensifying fluid disturbance (Tegladza et al., 2023). The bubble generation under different conditions was recorded in Fig. 9.

As shown in Fig. 9, under negative pressure conditions, the bubbles generated were numerous but small in size, which resulted mainly from dissolved gas release (Jun, 2023); under ultrasonic conditions, the bubbles were larger in size but fewer in number, predominantly cavitation bubbles; while under ultrasonic negative pressure synergistic conditions, the bubbles were not only the most numerous and largest in

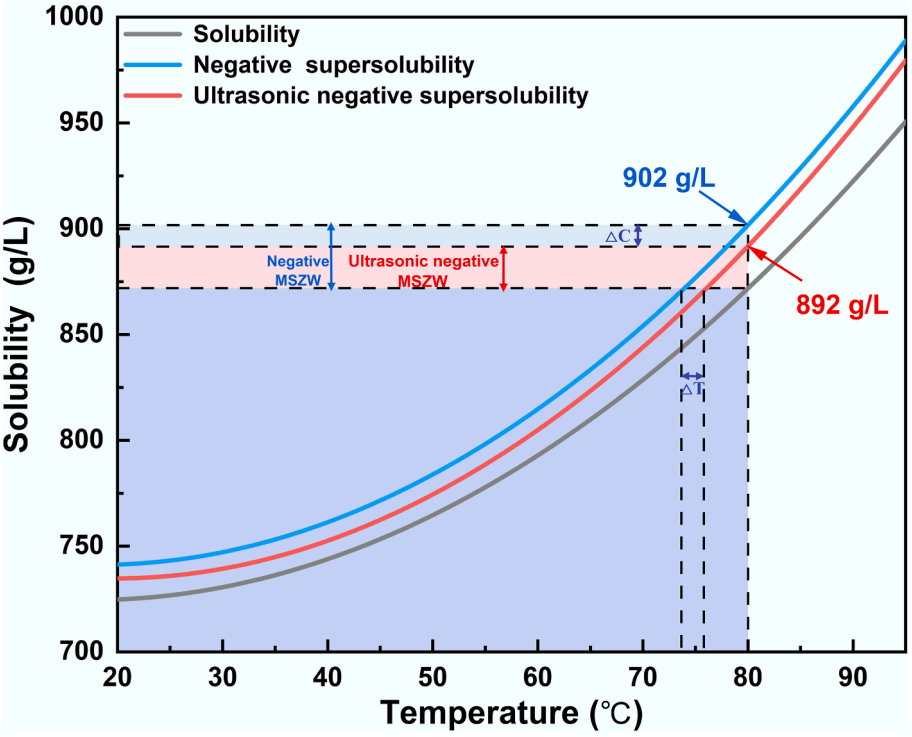

Fig. 8. Solubility curves and metastable zone width of ammonium sulfate under negative pressure and ultrasonic negative pressure conditions.

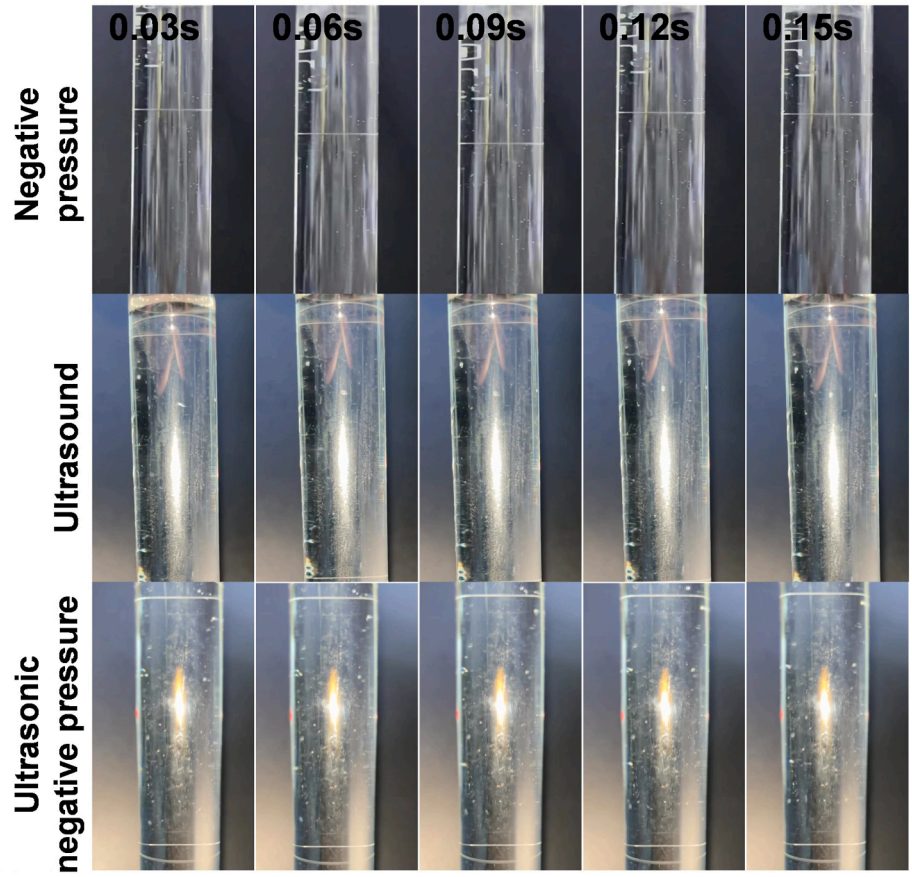

Fig. 9. Bubble generation under different conditions.

size, but also grew more rapidly. This is because negative pressure provides thermodynamic driving force for gas supersaturation, while ultrasound provides kinetic disturbance through high-frequency pressure oscillation, and their combined effect accelerates bubble growth.

Bubbles accelerate nucleation mainly through two mechanisms (Wohlgemuth et al., 2009). First, solvent evaporates into the bubbles, forming local supersaturation higher than the bulk in the interfacial region, thereby enhancing the crystallization driving force. Second, the bubble surface serves as a heterogeneous nucleation site, reducing the nucleation energy barrier. Therefore, nucleation is more likely to occur under ultrasonic negative pressure conditions. Bubbles under ultrasonic and ultrasonic negative pressure conditions can be classified into stable cavitation (inactive bubbles) and transient cavitation (active bubbles) based on their kinetic behavior (Wang et al., 2024). When the acoustic pressure amplitude exceeds a specific threshold, the expansion and compression processes of bubbles become unstable. Among them, stable cavitation is characterized by cavitation bubbles undergoing nonlinear oscillations over multiple acoustic cycles, eventually collapsing in a relatively gentle manner. Transient cavitation refers to cavitation bubbles rapidly expanding within one acoustic cycle and subsequently collapsing violently, accompanied by the generation of local high temperature and high pressure phenomena. As shown in Fig. 10(a), all experiments were performed on aluminum foil (approximately 4 cm × 4 cm, with an initial weight of approximately 0.0392-0.0423 g) at room temperature. The three conditions included negative pressure alone at 0.03 MPa, ultrasound alone at 180 W, and combined ultrasound (180 W) with negative pressure (0.03 MPa). The corresponding mass loss data (the difference in aluminum foil mass before and after treatment) are presented in Fig. 10(b). These data directly reflect the cavitation strength, as aluminum foil mass loss is a well-established measure

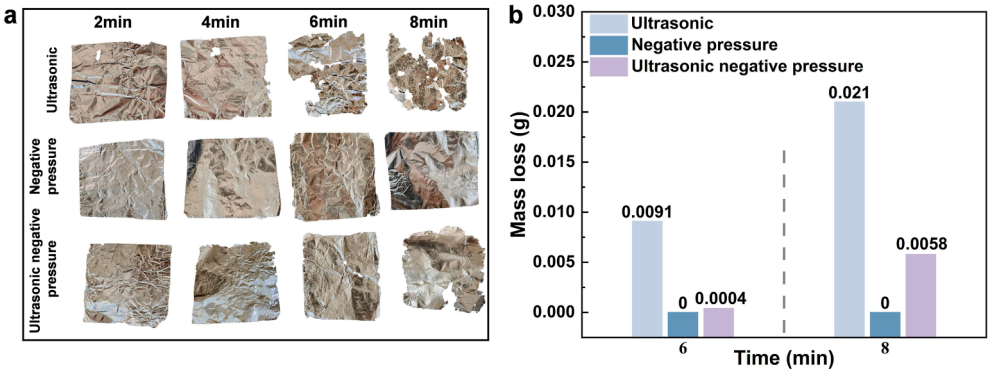

Fig. 10. (a) Erosion degree of aluminum foil under different conditions, (b) Mass loss of aluminum foil after treatment under different conditions.

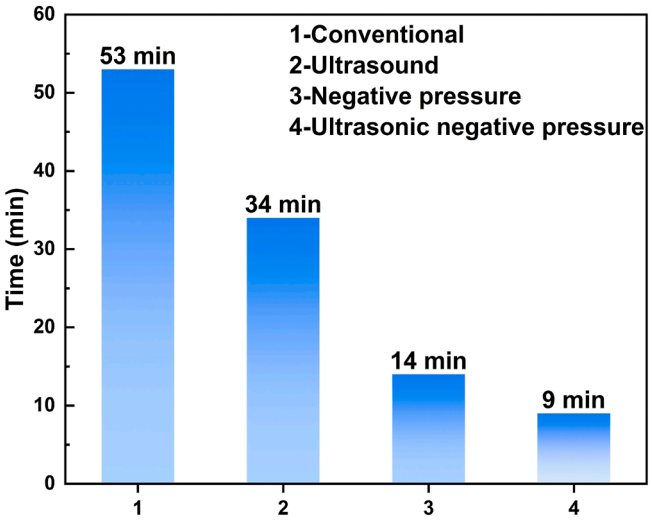

Fig. 11. Solid-liquid transition time under different conditions.

of cavitation erosion intensity where greater loss indicates more severe cavitation impacts (Saikova et al., 2026). Under negative pressure alone, the aluminum foil surface remained almost intact, with no measurable mass loss, indicating that cavitation was hardly generated. In contrast, under ultrasonic conditions alone, the foil surface exhibited progressively intensifying erosion pits over time, reflecting strong cavitation activity with numerous active bubbles. The mass loss was the largest. However, under the combined ultrasonic negative pressure conditions, the degree of aluminum foil erosion was relatively small, with very low mass loss, suggesting that the cavitation bubbles were predominantly inactive and that the cavitation effect was relatively mild. This avoids excessive cavitation-induced fragmentation of already formed nuclei or fine crystals during ultrasound, while simultaneously suppressing nuclei agglomeration under negative pressure conditions, thereby facilitating the stable progression of the nucleation process.

The time from the start of heating to the occurrence of crystal precipitation was recorded as the solid-liquid transition time. This time is equal to the sum of the solution heating time and the crystallization induction time. The solid-liquid transition times under different conditions are shown in Fig. 11. Under ultrasonic negative pressure conditions, the solid-liquid transition time was significantly shortened to only 9 min. Compared with negative pressure conditions, crystallization under ultrasonic negative pressure reduced the solid-liquid transition time by 35.7%, indicating faster nucleation speed under these conditions.

Scanning electron microscopy was employed to further investigate the morphological evolution of ammonium sulfate crystals during the crystallization process. The crystal morphologies at 5 min and 10 min after precipitation under negative pressure and ultrasonic negative pressure conditions (corresponding to crystallization times of 19 min and 24 min for negative pressure, and 14 min and 19 min for ultrasonic negative pressure) are shown in Fig. 12. Under conventional negative pressure, crystals exhibited a pronounced rod-like growth habit, which persisted over time (19-24 min). In contrast, in the ultrasonic negative pressure system, crystals appeared rod-like at 14 min, whereas at 19 min, numerous fine crystals dominated, suggesting that ultrasound-induced fragmentation of rod-like crystals promotes secondary nucleation. Consequently, the nuclei density is substantially increased, enhancing product yield within the same crystallization duration.

Viscosity is a key physical parameter influencing crystal nucleation and growth. During the nucleation stage, elevated viscosity increases the diffusion resistance of solute molecules and reduces the frequency of

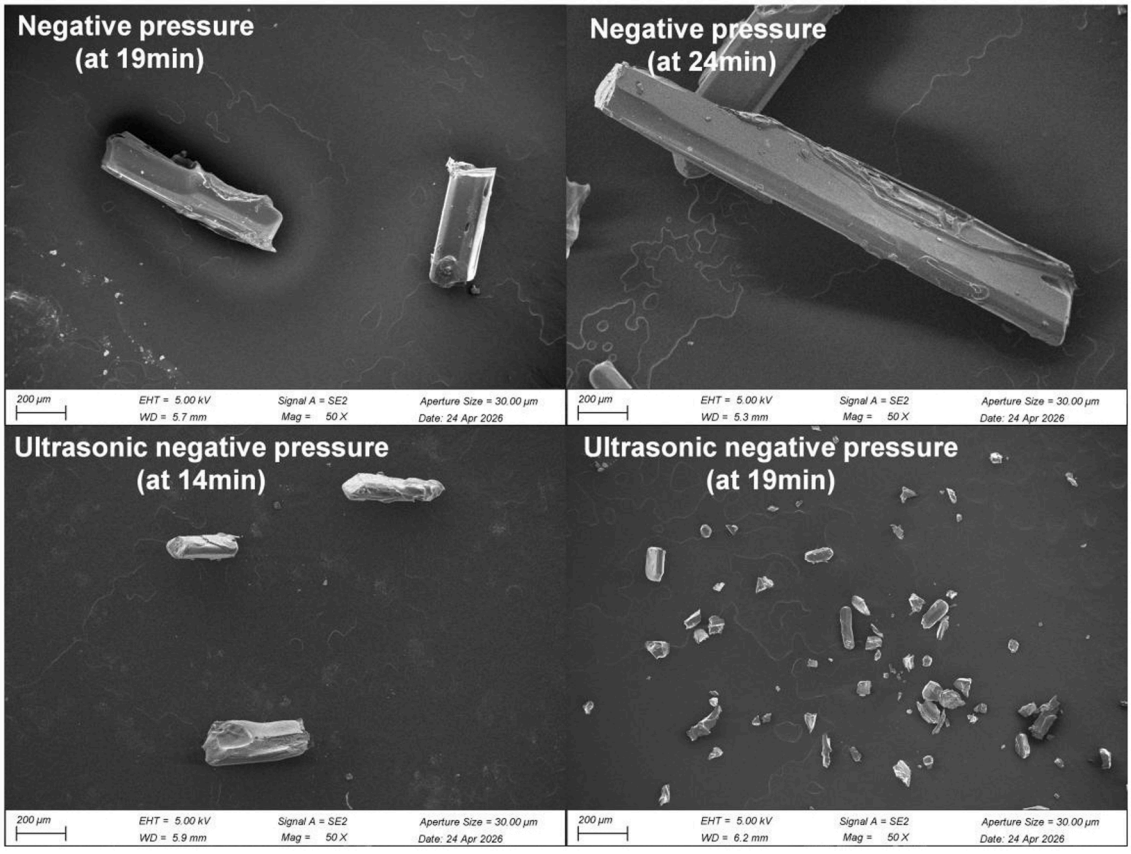

Fig. 12. Crystal morphological evolution during negative pressure and ultrasonic negative pressure crystallization.

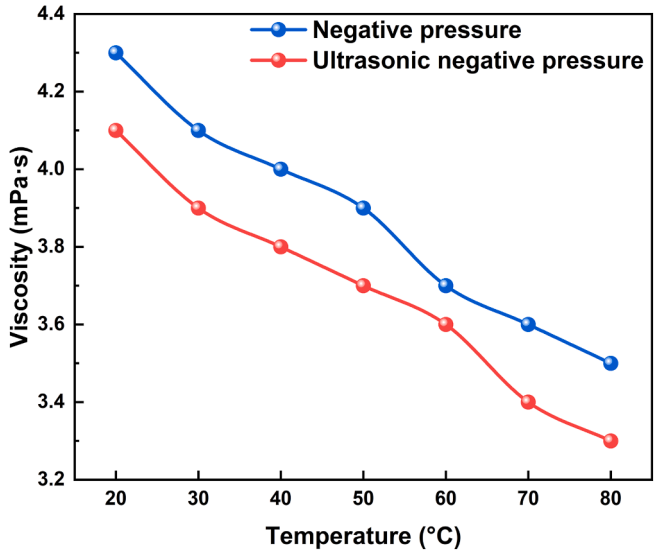

Fig. 13. Variation of solution viscosity with temperature under different reaction conditions.

effective intermolecular collisions, thereby suppressing primary nucleation and prolonging the crystallization induction period (Thieme & Rüssel, 2014). During the growth stage, excessive viscosity hinders both the diffusion of solutes from the solution to the crystal surface and the integration of growth units onto the crystal facets, resulting in a decreased crystal growth rate (Nicholson et al., 2023). High-frequency vibration of ultrasound induces forced vibration of liquid molecules, increasing molecular spacing and weakening intermolecular interactions through periodic compression and stretching, thereby reducing flow internal friction and decreasing viscosity (Bakrutheen et al., 2018). In addition, the collapse of ultrasonic cavitation bubbles generates localized transient high temperatures (approximately 5000 K), which intensify the thermal motion of solute and solvent molecules, weaken intermolecular van der Waals forces and hydrogen bonds, increase the average intermolecular distance, and thereby reduce the solution viscosity (Zhang et al., 2026). The variation of ammonium sulfate solution viscosity with temperature under different reaction conditions is shown in Fig. 13. Compared with negative pressure conditions, the viscosity of ammonium sulfate solution under ultrasonic negative pressure conditions was lower, with a 5.7% reduction at 80 °C. The enhanced solute diffusion capacity facilitates the migration of NH_4^+ and SO_4^{2-} ions toward crystal surfaces, thereby promoting rapid growth of ammonium sulfate crystals.

The mechanism of ultrasonic negative pressure enhanced ammonium sulfate crystallization is illustrated in Fig. 14. Under ultrasonic-negative pressure conditions, numerous bubbles are generated in the solution, providing abundant heterogeneous nucleation sites and enhancing local supersaturation driving force, thereby accelerating nucleation and shortening the solid-liquid transition time. Meanwhile, this approach avoids crystal damage caused by excessive mechanical stress under ultrasound alone as well as crystal agglomeration under negative pressure alone. Additionally, these conditions can reduce solution viscosity, accelerate solute diffusion, and promote crystal growth. Therefore, introducing ultrasound into the negative pressure evaporation crystallization process of ammonium sulfate can significantly shorten the crystallization time, improve the direct yield, and obtain ammonium sulfate crystals with higher crystallinity, more uniform particle size, and more regular morphology.

4. Conclusion

In this study, an ultrasonic negative pressure crystallization process for ammonium sulfate was proposed. The major conclusions are as follows:

(1) Compared with negative pressure crystallization, under optimal conditions, the yield of ammonium sulfate increased by 27.64 g, and the direct yield significantly improved by 36.80%.
(2) XRD and FTIR analyses indicated that this process effectively improved product crystallinity without altering the crystal structure of ammonium sulfate. SEM and particle size analysis further confirmed that the synergistic effect of ultrasonic negative pressure promoted more regular crystal morphology and more uniform particle size.
(3) The synergistic intensification mechanism of ultrasound and negative pressure was revealed. Compared with negative pressure crystallization alone, the introduction of ultrasound narrowed the MSZW by approximately 33%, lowering the nucleation energy barrier. Meanwhile, the abundant bubbles generated by ultrasonic cavitation provided numerous heterogeneous nucleation sites and local supersaturation driving forces, reducing the solid-liquid transition time by 35.7%. Furthermore, the introduction of ultrasound inhibited excessive growth, induced secondary nucleation, and increased crystallization yield, while reducing solution viscosity by 5.7%, thereby enhancing mass transfer and crystal growth.

Overall, this process effectively overcomes the problems of crystal agglomeration and broad particle size distribution inherent in traditional processes, and develops an efficient ammonium sulfate

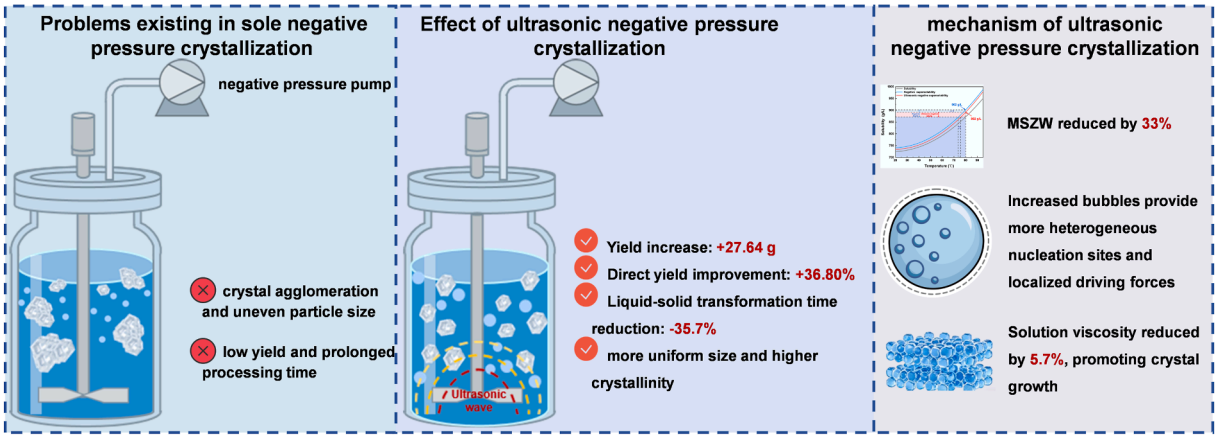

Fig. 14. Mechanism diagram of ultrasonic negative pressure enhanced ammonium sulfate crystallization.

crystallization process suitable for industrial production. However, industrialization still requires systematic resolution of engineering boundary conditions such as thermal stability of ultrasonic transducers, impurity sensitivity of industrial mother liquor, and material corrosion resistance. Combining process simulation with pilot-scale validation in the future is crucial for bridging laboratory achievements and industrial applications.

CRediT authorship contribution statement

Qian Zhang: Writing – original draft, Formal analysis. **Guang Fu:** Formal analysis. **Shuo Xu:** Formal analysis, Data curation. **Dongbin Wang:** Formal analysis. **Thiquynhxuan Le:** Writing – review & editing, Funding acquisition, Formal analysis, Conceptualization. **Libo Zhang:** Supervision, Resources.

Declaration of competing interest

The authors declare that they have no known competing financial interests or personal relationships that could have appeared to influence the work reported in this paper.

Acknowledgement

This work was financially supported by the National Foreign Experts Program of China (grant No. H20250152), Yunnan Province Key R&D Plan (grant No. 202403AK140009), and Yunnan Fundamental Research Project (grant No. 202501BN070001-010).

References

Aquilanti, V., Borges, E. P., Coutinho, N. D., Mundim, K. C., & Carvalho-Silva, V. H. (2018). From statistical thermodynamics to molecular kinetics: The change, the chance and the choice. *Rendiconti Lincei, 29*(4), 787–802.

Bakrutheen, M., Iruthayarajan, M. W., & Narayani, A. (2018). Influence of ultrasonic waves on viscosity of edible natural esters based liquid insulation. *IEEE Transactions on Dielectrics and Electrical Insulation, 25*(5), 1628–1635.

Devos, C., Bampouli, A., Brozzi, E., Stefanidis, G. D., Dusselier, M., Van, G. T., & Kuhn, S. (2025). Ultrasound mechanisms and their effect on solid synthesis and processing: A review. *Chemical Society Reviews, 54*(1), 85–115.

Dong, J., Wu, Y., Wang, J., Wang, S., & Wen, J. (2025). Investigation of the strengthening mechanisms and laws of ultrasound fields on the crystallization process of Paraxylene. *Powder Technology, 452*, Article 120518.

Edward, Wongprasert, T., Bunyakanchana, T., Siripitakpong, P., Supabowornsathit, K., Vilaivan, T., & Suppavorasatit, I. (2023). Cricket protein isolate extraction: Effect of ammonium sulfate on physicochemical and functional properties of proteins. *Foods, 12*(21), Article 4032.

Gao, H., Pei, K., Hu, G., Liu, W., Meng, A., Wang, H., Shao, H., & Li, W. (2022). The influence of pressure on the acoustic cavitation in saturated CO2-expanded N, N-dimethylformamide. *Ultrasonics Sonochemistry, 83*, Article 105934.

Guo, J., Yu, H., Wang, D., & Fan, L. (2026). Cavitation-enhanced carbonation for nano-ZnO synthesis via an ultrasonic-jet coupled reactor: Machine learning prediction and multi-objective optimization using a genetic algorithm. *Ultrasonics Sonochemistry, 129*, Article 107859.

Hu, A., Zheng, J., & Qiu, T. (2006). Industrial experiments for the application of ultrasound on scale control in the Chinese sugar industry. *Ultrasonics Sonochemistry, 13*(4), 329–333.

Ileri, B., Ayyildiz, O., & Apaydin, O. (2015). Ultrasound-assisted activation of zero-valent magnesium for nitrate denitrification: Identification of reaction by-products and pathways. *Journal of Hazardous Materials, 292*, 1–8.

Jun, Y.-D. (2023). Degassing dissolved oxygen through bubbling: The contribution and control of vapor bubbles. *Applied Sciences, 11*(11), Article 3158.

Kim, S., Kim, T., Lee, J., Cho, S. H., Kim, T. E., & Lee, Y. S. (2026). Vacuum-controlled solvent evaporation for morphological engineering of wide-bandgap perovskite films. *ACS Applied Materials & Interfaces, 18*, 3863–3871.

Kocks, C., Krekel, C. M., Gausmann, M., & Jupke, A. (2021). Determination of the metastable zone width and nucleation parameters of succinic acid for electrochemically induced crystallization. *Crystals, 11*(9), Article 1090.

Li, S., Li, Q., Zhu, F., Song, H., Wang, C., & Guan, X. (2022). Effect of vacuum combined ultrasound treatment on the fine structure and physiochemical properties of rice starch. *Food Hydrocolloids, 124*, Article 107198.

Liu, D., Jiang, X., Wang, H., Chen, H., Lu, Y.-B., Dong, S., Ning, Z., Wang, Y., Wu, Z., & Ling, Z. (2024). Perovskite single crystals by vacuum evaporation crystallization. *Advanced Science, 11*(22), Article e2400150.

Liu, L., Wang, M., Liu, Y., Bi, Q., & Liu, Y. (2015). Heat and mass transfer characteristics of evaporation and salt crystallization process of a saline droplet during depressurization. *CIESC Journal, 66*(7), 2426–2432.

Min, H.-S., Kim, H.-G., & Kim, J.-H. (2022). Ultrasound-negative pressure cavitation extraction of paclitaxel from Taxus chinensis. *Korean Journal of Chemical Engineering, 39*(2), 398–407.

Mohod, A. V., & Gogate, P. R. (2018). Improved crystallization of ammonium sulphate using ultrasound assisted approach with comparison with the conventional approach. *Ultrasonics Sonochemistry, 41*, 310–318.

Myerson, A. S., Erdemir, D., & Lee, A. Y. (2019). *Handbook of industrial crystallization*.

Nicholson, S. T., Roberts, K. J., Izumi, T., & Lai, X. (2023). Characterization of mass transfer within the crystal-solution boundary layer of l-alanine {120} faces using laser interferometry during growth and dissolution. *Crystal Growth & Design, 23*(4), 2755–2769.

Pei, S., Zhang, A. M., Liu, C., Zhang, T., Han, R., & Li, S. (2025). Influence of ambient temperature on cavitation bubble dynamics. *Journal of Fluid Mechanics, 1023*, Article A28.

Peng, J., Yang, Z., & Lian, P. (2024). Process optimization and crystallization kinetics of ammonium sulfate from wet ammonia-based desulfurization. *Environmental Progress & Sustainable Energy, 43*(2), Article e14310.

Penha, F. M., Zago, G. P., Nariyoshi, Y. N., Bernardo, A., & Seckler, M. M. (2018). Simultaneous crystallization of NaCl and KCl from aqueous solution: Elementary phenomena and product characterization. *Crystal Growth & Design, 18*(3), 1645–1656.

Qu, X., Tang, Y., Li, M., Liu, D., Gao, S., & Yin, H. (2022). Mechanisms of the ammonium sulfate roasting of spent lithium-ion batteries. *Global Challenges, 6*(12), Article 2200053.

Saikova, S., Nemkova, D., & Krolikov, A. (2026). Effect of experimental parameters on cavitation dose in ultrasonic baths via modified aluminum foil test. *Molecules, 31*(8), Article 1291.

Seo, H.-B., & Lee, S.-Y. (2023). High-concentration nanobubble generation by megasonic cavitation and atomization. *Colloid and Interface Science Communications, 52*, Article 100687.

Shao, G., He, Z., Xiao, W., He, G., Ruan, X., & Jiang, X. (2022). On-line monitoring and analysis of membrane-assisted internal seeding for cooling crystallization of ammonium persulfate. *Chemical Engineering Science, 263*, Article 118081.

Song, L., Zeng, Y., Liang, M., Di, H., Liu, J., Yang, K., & Zhang, L. (2023). Process optimization and mechanism of high-efficiency germanium extracting from zinc oxide dust containing germanium enhanced by ultrasound. *Chemical Engineering and Processing: Process Intensification, 191*, Article 109439.

Tegladza, I. D., Lin, G., Liu, C., & Gu, X. (2023). Control of crystal nucleation, size and morphology using micro-/nanobubbles as green additives. *Separation and Purification Technology, 311*, Article 122967.

Thieme, K., & Rüssel, C. (2014). Nucleation inhibitors—the effect of small concentrations of Al2O3, La2O3 or TiO2 on nucleation and crystallization of lithium disilicate. *Journal of the European Ceramic Society, 34*(15), 3969–3979.

Vishwakarma, R. S., & Gogate, P. R. (2017). Intensified oxalic acid crystallization using ultrasonic reactors: Understanding effect of operating parameters and type of ultrasonic reactor. *Ultrasonics Sonochemistry, 39*, 111–119.

Wang, D., Miao, W., Fu, M., Tran, V., Xv, T., Zhang, Q., Le, T., & Zhang, L. (2025). Ultrasound-enhanced crystallization of sodium stannate: Mechanisms of nucleation and growth control. *Journal of Materials Research and Technology, 39*, 2009–2020.

Wang, H., Wang, X., Wang, Y., Wang, D., Hu, K., Zhong, W., & Guo, Z. (2024). Influence of ammonium sulfate leaching agent on engineering properties of weathered crust elution-deposited rare earth ore. *Acta Geotechnica, 19*(4), 1–22.

Wang, T., Xie, Y., Miao, W., Sun, K., Ji, Y., Duoc, T. V., Le, T., & Zhang, L. (2025). Improvement of molybdenum trioxide quality via ultrasound-enhanced water washing: Targeted removal of structural potassium under neutral conditions. *Journal of Cleaner Production, 523*, Article 146465.

Wang, B., Zeng, T., Shang, J., Tao, J., Liu, Y., Yang, T., Ren, H., & Hu, G. (2024). Bubble dynamics model and its revelation of ultrasonic cavitation behavior in advanced oxidation processes. *Journal of Water Process Engineering, 63*, Article 105470.

Weis, D. D., & Ewing, G. E. (1996). Infrared spectroscopic signatures of (NH4)2SO4 aerosols. *Journal of Geophysical Research: Atmospheres, 101*(D13), 18709–18720.

Wohlgemuth, K., Kordylla, A., Ruether, F., & Schembecker, G. (2009). Experimental study of the effect of bubbles on nucleation during batch cooling crystallization. *Chemical Engineering Science, 64*(19), 4155–4163.

Xing, Y., Wei, Y., Yuan, H., & Zhu, N. (2026). Promote heterogeneous nucleation of struvite in livestock wastewater by regulating the surface properties of suspended particles with ultrasound-assisted pretreatment. *Water Research, 289*, Article 124858.

Xu, H., Fu, G., Phan, D., Xiang, L., Le, T., & Zhang, L. (2024). Evaporating crystallization effect of ammonium sulfate at atmospheric pressure under the action of ultrasound. *Ultrasonics Sonochemistry, 106*, Article 106896.

Xu, T., Wang, D., Lenh, P. D., Xiang, L., Wang, T., Le, T., & Zhang, L. (2025). Intermittent ultrasound-enhanced morphology regulation and process intensification of ammonium sulfate crystallization in desulfurization solution. *Journal of Environmental Chemical Engineering, 13*(6), Article 120360.

Xu, L., Yao, X., & Shen, Y. (2024). Dynamic modeling of cavitation bubble clusters: Effects of evaporation, condensation, and bubble-bubble interaction. *Chinese Physics B, 33*(4), 526–535 (in Chinese).

Yan, S., Dong, X., Jiang, H., Liu, Y., Han, Y., Guo, T., Zhang, Y., Li, J., & Yan, Q. (2024). Oil-coated ammonium sulfate improves maize nutrient uptake and regulates nitrogen leaching rates in sandy soil. *Agronomy, 14*(7), Article 1463.

Yang, S., Yang, H., Wang, F., Song, X., Cui, S., Feng, J., Ning, P., & Jia, L. (2025). Efficient recovery of zinc resources from high chloride zinc slag via ammonia-ammonium sulfate-ammonium persulfate system. *Separation and Purification Technology, 362*, Article 131765.

Yang, Z., Zuo, Y., Dai, L., Zhang, L., Yu, Y., & Zhou, L. (2023). Effect of ultrasonic-induced selenium crystallization behavior during selenium reduction. *Ultrasonics Sonochemistry, 95*, Article 106392.
Zhang, J., Yu, R., Ren, J., Cui, X., Ye, L., & Zhu, X. (2026). Molecular dynamics and energy analysis of ultrasonic cavitation effects on aged asphalt. *Ultrasonics Sonochemistry, 126*, Article 107765.
Zhao, Q., Yang, L., Yao, C., & Chen, G. (2023). Ultrasonic enhanced continuous crystallization: Induction time and process control. *Industrial & Engineering Chemistry Research, 62*(47), 20083–20095.
Zheng, D., Xu, M., Wang, J., Ma, Y., Tian, Y., Shen, Y., Wu, X., & Yang, M. (2023). Nonisothermal crystallization kinetics of potassium chloride produced by stirred crystallization. *Journal of Crystal Growth, 603*, Article 127035.
Zhong, X., Huang, C., Chen, L., Yang, Q., & Huang, Y. (2022). Effect of ultrasound on the kinetics of anti-solvent crystallization of sucrose. *Ultrasonics Sonochemistry, 82*, Article 105886.